Polym. Bull. (2011) 67:159–175
DOI 10.1007/s00289-010-0438-z

ORIGINAL PAPER

Cell-culture compatible silk fibroin scaffolds concomitantly patterned by freezing conditions and salt concentration

Frédéric Byette · Frédéric Bouchard · Christian Pellerin · Joanne Paquin · Isabelle Marcotte · Mircea A. Mateescu

Received: 17 August 2010 / Revised: 1 December 2010 / Accepted: 30 December 2010 /
Published online: 22 January 2011

Abstract The morphology of freeze-dried silk fibroin 3D-scaffolds was modified by varying both the NaCl concentration and the freezing temperature of the silk fibroin solution prior to lyophilization. Scanning electron micrographs showed that slow freezing at −22 °C generated sponge-like interconnected porous networks, whereas fast freezing at −73 °C formed stacked leaflet structures. The presence of millimolar NaCl (50–250 mM) increased the porosity of the scaffolds and generated small outgrowths at their surface, depending on the freezing regime. Our results suggest that the morphological differences seen between the materials likely depend on ice and NaCl hydrate crystal nucleation and growth mechanisms. Infrared spectroscopy and X-ray diffraction analyses revealed that the salt concentration and freezing conditions induced no structural changes in fibroin. The seeding of P19 embryonic carcinoma cells showed that the presence of salt and freezing conditions influenced the cell distribution into the scaffolds, with salt addition increasing the access of cells to deeper regions.

F. Byette · F. Bouchard · J. Paquin · I. Marcotte · M. A. Mateescu
Département de Chimie, Pharmaqam/NanoQAM, Université du Québec à Montréal, C.P. 8888, Montréal, QC H3C 3P8, Canada

C. Pellerin
Département de chimie, Université de Montréal and Center for Self-Assembled Chemical Structures (CSACS), Montréal, QC H3C 3J7, Canada

I. Marcotte (✉) · M. A. Mateescu (✉)
Department of Chemistry, Université du Québec à Montréal, P.O. Box 8888, Downtown Station, Montreal, QC H3C 3P8, Canada
e-mail: marcotte.isabelle@uqam.ca

M. A. Mateescu
e-mail: mateescu.m-alexandru@uqam.ca

Keywords Silk fibroin · Scaffold · Cell culture · Freeze-drying · Crystal nucleation and growth · Sodium chloride concentration · Freezing temperature · Mechanical properties · Spectroscopic characterization

Introduction

With the continuously growing interest in tissue engineering, there is an increasing need for porous three dimensional (3D) polymeric scaffolds to mimic the extracellular matrix of natural tissues and to promote cell migration, adherence, and proliferation into the structure [1, 2]. An interconnected porous network with appropriate pore size is essential to foster the transport of nutrients and wastes but also to favor cell migration into the structure and the formation of new tissue ingrowths when implanted into an organism [3–5]. Numerous synthetic and natural polymers have been investigated for the development of scaffolds as potential biomaterials, including silk [6, 7], polylactic acid, polyglycolic acid and their copolymers [2, 8], chitosan [9], collagen [10], alginate [3], poly(alpha-hydroxy) acids [11], and agarose [12]. The nature of the polymeric material used to prepare scaffolds is critical since it must be biocompatible and possess adequate mechanical properties to support tissue function and integration at the implantation site. In several applications, it should also be biodegradable at a rate comparable with the growth of new tissue [1]. Considering their amino acid or sugar-based structures, natural biopolymers have the advantages of biocompatibility and biodegradability when compared to most of the synthetic ones [13].

Despite the commercial availability of several materials and the constant progress made in controlling their mechanical characteristics, there is still a need for hypoallergenic biomaterials for tissue healing. Silkworm silk fibroin is a naturally occurring protein material that has been used for centuries in medicine as suture threads [14, 15]. Silk fiber from the *Bombyx mori* silkworm cocoon consist of two fibroin threads (core) surrounded by a sheath of sericin, a gummy water-soluble protein [14, 16]. The silk fibroin is formed of a single disulfide bridged complex composed of two polypeptide subunits of ca. 350 and 25 kDa, to which a glycoprotein of about 30 kDa associates primarily by hydrophobic interactions [17, 18]. These proteins have a highly repetitive amino acid sequence mainly composed of glycine (45%), alanine (30%), and serine (12%) residues [15, 19]. The particular sequence of these amino acids with small side chains leads to the formation of hydrophobic domains, thus allowing the formation of thick packs of hydrogen-bonded anti-parallel β-sheets [15, 19].

Silkworm silk fibroin is a good candidate for biomaterial development because of its impressive mechanical properties, biocompatibility, and biodegradability [14, 20, 21]. A variety of materials have already been processed from solubilized fibroin, including films [22, 23], gels [15], beads [24], electrospun fibers [25], and scaffolds [15]. Many routes have been explored to modulate the physical aspect of silk fibroin scaffolds. Among these, particulate leaching, gas foaming, electrospinning, freeze-thawing, and freeze-drying procedures have shown their efficiency to modify and template the morphology of the resulting materials [1, 5, 6, 15, 16, 26–29]. The use

of NaCl as porogen renders the leaching process biologically friendly as it is readily soluble in water. Also, the saturation of fibroin solutions with NaCl is known to induce a predominant β-sheet molecular structure in the resulting 3D scaffolds, thus yielding water insoluble porous materials [1]. The freezing of water slurries prior to freeze-drying is an adaptable method for both the template formation (freezing of water) and the template removal (sublimation of ice). The ice crystals formed during the freezing process create a pattern in the material that is maintained after freeze-drying. This approach offers versatility of structural modification since the freezing process can be conducted such as to control ice crystal size and growth [3, 9, 12, 30, 31]. More specifically, the cooling rate, the freezing temperature, and the initial concentration of the polymeric slurries, all affect the crystallization kinetics and, thus, the final morphology of freeze-dried scaffolds.

The modification of freezing conditions and the addition of NaCl crystals as porogens were methods used independently for scaffolds processing [1, 6]. It is noteworthy that the porosity originating from a salt treatment was controlled by the size of the NaCl crystals added at saturation in fibroin slurries. In contrast with this method, the present work focused on the simultaneous variation of freezing and salt conditions using diluted NaCl solutions. This strategy was adopted with the aim of developing an accessible low-cost technique to design scaffolds with adaptable morphologies, thus fulfilling the spatial needs of different cells when used as cell-culture support. The resulting materials were evaluated in terms of their morphology, mechanical properties, and molecular structure after methanol treatment. Their suitability for cell-culture application was verified using model P19 carcinoma stem cells.

Materials and methods

Preparation of silk fibroin aqueous solution

Cocoons of *Bombyx mori,* purchased from Tajima Shoji Co. Ltd (Yokohama, Japan), were boiled for 60 min in a 0.02 M Na_2CO_3 aqueous solution, then filtered and rinsed with hot distilled water to remove the sericin and wax coating from the silk fibroin threads. This process was repeated three times. The cleansed silk fibroin was then dissolved in a 9.3 M LiBr solution (1 g fibroin/dL) at 50 °C for 4 h. This solution was dialyzed for 3 days against distilled water using cellulose membrane tubing (MWCO 3500, Spectra/Por, Spectrum Laboratories Inc., Rancho Dominguez, CA). The final concentration of silk fibroin in the aqueous solution was about 3% (w/v), as determined by weighing the remaining solid after drying.

Silk fibroin scaffolds processing

Silk fibroin scaffolds were prepared by mixing a constant volume of the silk fibroin solution with an equivalent volume of various aqueous NaCl solutions. The final NaCl concentrations ranged from 0 to 250 mM. 3 mL of the resulting solutions were individually poured into Corning® 12-well polystyrene cell-culture plates with

a bottom thickness of 1.27 mm. Fast freezing was carried out by placing the covered plates on the shelves of a freezer at −73 °C while slow freezing conditions were obtained by enclosing covered plates in a polystyrene box at −22 °C to prevent rapid ice crystal nucleation. After 24 h in freezers, the frozen solutions were lyophilized for 3 days. The resulting scaffolds were treated with methanol for 1 h to induce water insolubility [32], immersed in distilled water for 24 h to remove the salt and traces of solvent, and finally air dried in an oven at 50 °C before utilization and characterization.

Swelling ratio and water uptake measurements

The scaffolds were immersed in distilled water for 24 h. The excess of water was removed and the weight of the wet samples (W_s) was measured. Samples were then dried at 50 °C overnight before determining their dry weight (W_d). The swelling ratio and water content in the scaffold were calculated as follows:

$$\text{Swelling ratio} = (W_s - W_d)/W_d \quad (1)$$

$$\text{Water uptake } (\%) = [(W_s - W_d)/W_s] \times 100 \quad (2)$$

Mechanical properties

Unconfined compression tests were performed on an Instron 3366 (Norwood, MA, USA) testing frame equipped with a 10 N load cell. The scaffolds were hydrated in 0.1 M Phosphate Buffer Saline (PBS) and submerged in a temperature-controlled Biopuls bath (37 ± 0.3 °C) filled with PBS for at least 2 min prior to testing. A strain control mode was used, with a crosshead displacement rate of 5 mm/min. The compressive stress and strain were calculated using the cross-sectional area (based on the sample casting size) and the sample height (measured automatically at a 0.02 N tare load). The elastic modulus was calculated by applying a least-squares fitting typically between 5 and 10% strain, based on the new sample height measured automatically. The compressive yield strength was determined using an offset-yield approach. A line was drawn parallel to the modulus line, but offset by 0.5% of the sample gauge length. The corresponding stress value at which the offset line crossed the stress–strain curve was defined as the compressive yield strength of the scaffold.

Scanning electron microscopy (SEM) and X-ray diffraction (XRD)

The scaffolds were cut axially through the center using a razor blade and images of the cross-sectioned surfaces were acquired using a HITACHI S-4300SE/N VP-SEM (Toronto, ON, Canada) equipped with a Schottky field emission gun operating at 15 kV. The XRD patterns of freeze-dried scaffolds were obtained on a Bruker D8 Discover diffractometer (Madison, WI, USA) using a Hi-Star area detector and a Cu K_α radiation source ($\lambda = 1.541838$ Å) operating at 40 kV and 40 mA. The distance between the detector and the sample was 8.0 cm.

Attenuated total reflectance (ATR) Fourier transform infrared (FT-IR) spectroscopy

Infrared spectra of the scaffolds were obtained using a Bruker Tensor 27 spectrometer (Billerica, MA, USA) with a liquid nitrogen-cooled mercury–cadmium–telluride detector and a Pike MIRacle single reflection ATR accessory. Each spectrum was acquired by averaging 185 scans at a 4 cm^{-1} resolution. Spectra were baseline-corrected using GRAMS/AI v.7.00 (Thermo Fisher Scientific, Waltham, MA, USA).

Cell culture

P19 carcinoma embryonic stem cells were routinely cultured at 37 °C in a propagation medium consisting of alpha-modified Eagle's minimum essential medium (αMEM; Invitrogen Life Technologies, Burlington, ON, Canada) supplemented with 10% heat-inactivated fetal bovine serum, 50 U/mL penicillin, and 50 μg/mL streptomycin under a humidified atmosphere of 5% CO_2. Passages were done every 2 days using trypsin and EDTA to detach the cells [33]. Before being seeded with cells, the silk fibroin scaffolds were cross-sectioned through the radial axis into two pieces, sterilized by autoclaving at 121 °C for 30 min, and hydrated with sterile PBS overnight. P19 cells were loaded with 5(6)-carboxyfluorescein diacetate *N*-succinimidyl ester (CFSE; Sigma, Oakville, ON, Canada) before seeding. For this, trypsinized cells were incubated for 15 min in PBS containing 30 μM of the fluorescent dye, washed with PBS, suspended in the propagation medium, and seeded onto scaffolds. This was achieved by depositing a 100 μL-suspension containing 1.5 millions cells onto the cross-sectioned surface of each scaffold using an automated micropipette. After a delay of 40 min to initiate cell penetration, the propagation medium was added to cover the scaffolds and culture was allowed for 24 h.

Confocal laser scanning microscopy

Distribution of cells onto and into the scaffolds was examined after the 24 h of culture using a BioRad MRC1024 confocal laser scanning microscope (Microscience, Cambridge, MA, USA). Prior to examination, silk fibroin scaffolds were transferred to new microwells, and 400 μL of a PBS solution containing propidium iodide (100 μg/mL) were gradually deposited onto the cell-seeded side of each scaffold. Propidium iodide impregnated the scaffolds, which were then placed on a microscope slide, the cell-seeded side in contact with the slide surface. Microscope examination and Z-scanning through the first 100 μm from the slide surface was done using 488 and 535 nm as the excitation and emission wavelengths, respectively. The Z sections were clubbed together and reconstituted into 3D images with the Zeiss LSM Image Browser software (Carl Zeiss Canada Ltd., Toronto, ON, Canada).

Results and discussion

Scaffolds processing and morphology

The freezing regime of material slurries such as those of silk, ceramics, and carbon nanotubes was shown to critically affect the resulting morphology of lyophilized materials [8, 16, 27, 31, 34]. On the other hand, the size of NaCl crystals saturating the fibroin slurries can be used to control porosity [1]. In the present work, we have exploited the simultaneous influence of the freezing conditions and concentration of NaCl solutions on the silk fibroin scaffold morphology to prepare 3D-matrices for cell-culture applications. Moreover, we have been focusing on extreme cases in the scaffolds processing set-ups in order to better evidence the morphological differences. For this purpose, the scaffolds have been prepared either by slow freezing of fibroin solutions enclosed in polystyrene box at −22 °C, or by fast freezing in direct contact with the freezer plate at −73 °C. The NaCl concentrations into the frozen fibroin solutions were relatively low, ranging from 0 to 250 mM (Fig. 1).

As a result of the slow cooling at −22 °C in the polystyrene box, solutions gradually became cloudy as ice crystals were forming. The resulting scaffold structures obtained by varying the salt concentration before the cooling are revealed on SEM micrographs (Fig. 2). Scaffolds processed without salt addition exhibited a dense and well-packed network of silk fibroin. As the concentration of NaCl added to the fibroin slurry increased, the network became more interconnected with more pores seen through the samples on SEM micrographs, as better evidenced when higher salt concentrations were used (Fig. 2j).

The final morphology of the scaffolds can be explained by the ice crystal formation during freezing. The eutectic temperature for the NaCl/water binary system is −21.1 °C [35–37]. Above this temperature, pure water freezes and excludes NaCl (and fibroin) toward the liquid phase. Because of the polystyrene shielding, the eutectic point (being near the nominal freezing temperature of

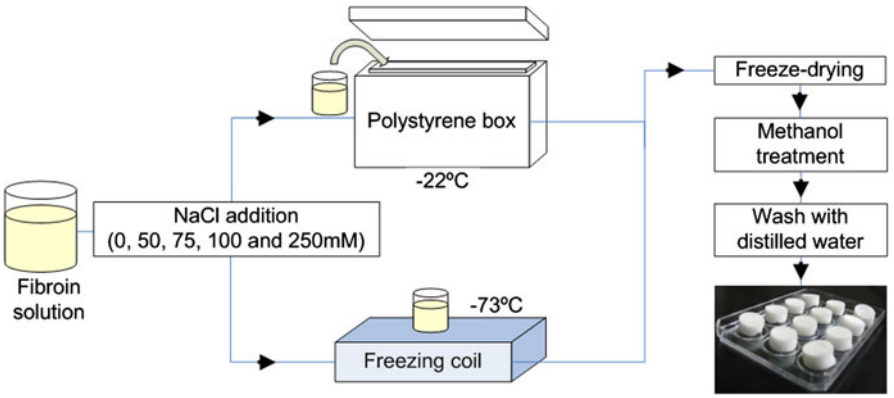

Fig. 1 Scaffolds processing flowchart

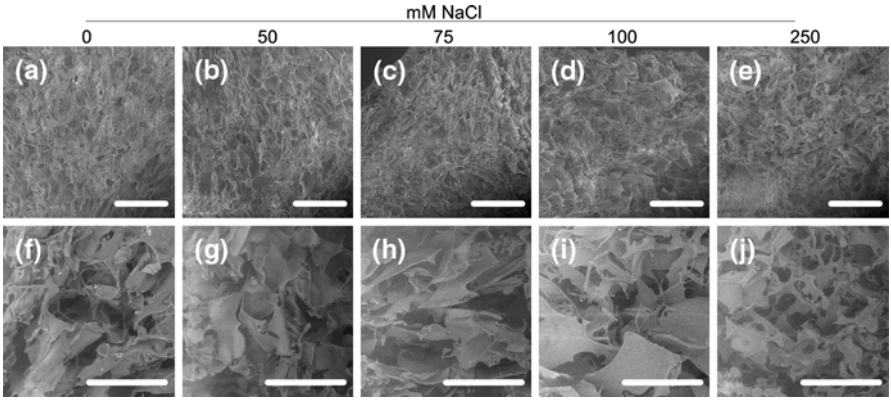

Fig. 2 SEM micrographs of cross-sectioned freeze-dried scaffolds prepared by freezing at −22 °C with or without NaCl addition. The *upper* (**a–e**) and *lower* (**f–j**) *row scale bars* are 500 and 200 μm, respectively

−22 °C) is slowly reached, and so is the transition across the liquid–solid equilibrium line to achieve complete freezing of the solution along with NaCl hydrate crystals formation. As pure water crystals are formed, a brine fibroin-enriched solution is created and favors protein–protein interactions. The slow freezing process, therefore, results in an entangled porous fibroin network (Fig. 2j). The coexistence of a NaCl-enriched solution and ice crystals allows the formation of different structures within the fibroin scaffolds depending on the salt concentration employed because it affects the size of the water and NaCl crystals (Fig. 2)

In contrast to the experiments done at −22 °C, the scaffolds prepared at −73 °C were in direct contact with the freezer surface and the cold atmosphere. Figure 3 shows SEM micrographs of the resulting scaffolds as a function of salt concentration in the solution. All scaffolds were composed of partially oriented

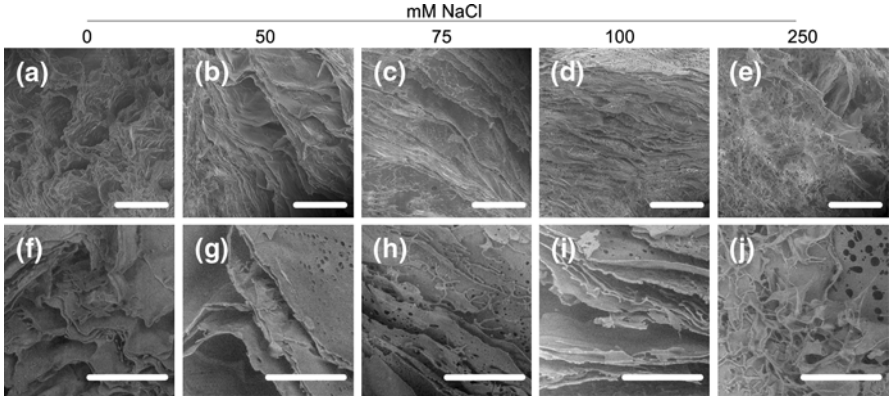

Fig. 3 SEM micrographs of cross-sectioned freeze-dried scaffolds prepared by freezing at −73 °C with or without NaCl addition. The *upper* (**a–e**) and *lower* (**f–j**) *row scale bars* are 500 and 200 μm, respectively

stacked leaf-like structures of silk fibroin. The leaflets appear as being more closely packed in samples with no or low salt concentration. With increased salt concentration, micropores can be observed through the fibroin leaflets, as evidenced in Figs. 3f–j and 4a. It is worth noting that formation of fibroin scaffolds arranged almost entirely into stacked leaflets has rarely been mentioned in the literature. When observed, such leaflets were not abundant and rather dispersed into the scaffolds [6, 38]. Finger-like structures were also formed on the surface of some leaflets (Fig. 4b, c). The increasing NaCl concentrations created more micropores and budding structures within the scaffolds. At the highest salt concentration (250 mM), the scaffold constructs looked less ordered as a result of increased porosity and number of finger-like outgrowths (Fig. 4d).

It is known that higher cooling rates (i.e. lower crystallization temperatures) produce more small ice crystals due to supercooling, and that nucleation mainly

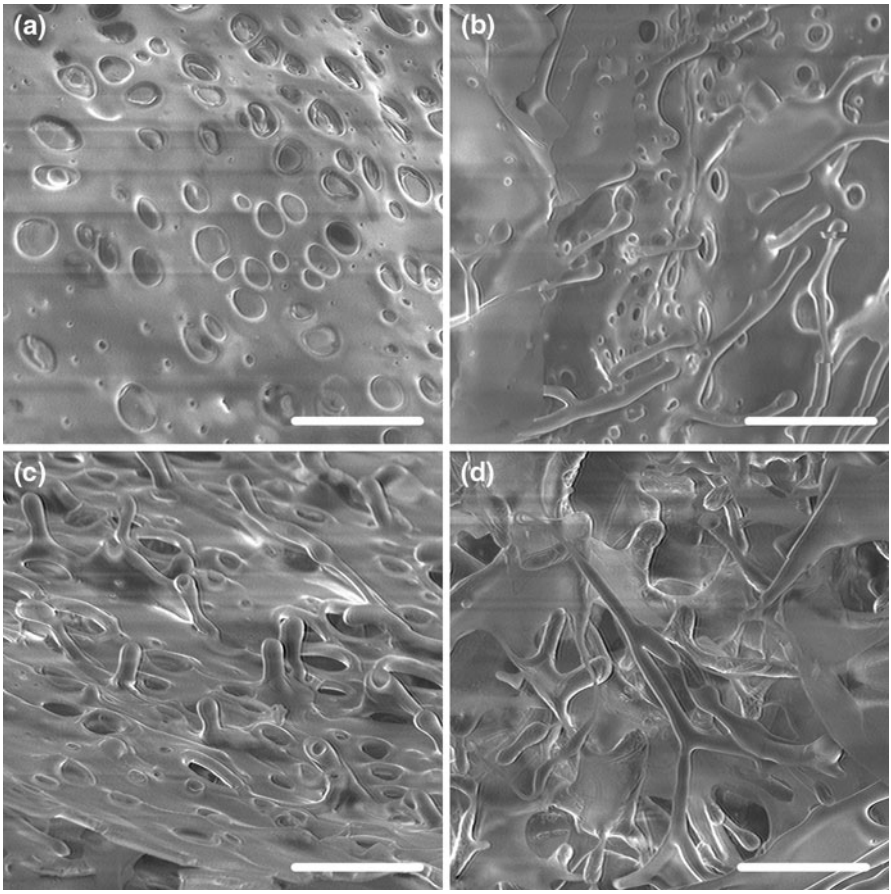

Fig. 4 High magnification SEM micrographs of cross-sectioned freeze-dried scaffolds prepared by freezing at −73 °C with **a** 50, **b** 75, **c** 100, and **d** 250 mM NaCl added before freezing. *Scale bars* represent 50 μm

occurs in zones directly in contact with the refrigerant [39, 40]. This causes a directional growth of the ice crystals across the slurry, starting at the sites of contact with the cold surface and developing as walls and pillars toward the center of the sample [30]. The solubilized fibroin and salt ions are expulsed by the crystallization front and can concentrate between these walls, leading to viscous concentrated slurry zones. As the cooling process continues, the water bound to salt ions and fibroin nucleates and smaller ice crystals can grow in the concentrated fibroin and salt slurry zone, leading to a final liquid–solid phase separation. Therefore, the process generates leaf-like structures between ice walls as well as the apparition of budding features on and between the fibroin leaflets (Fig. 4). As reported by Nam et al. [41] for poly(D,L-lactic-*co*-glycolic acid) foams, the formation of these irregular outgrowths suggests that the thermally induced phase separation mainly occurs by a nucleation and growth mechanism. The generation of micropores in the leaf-like structures in the presence of salt may be the result of the exclusion of salt ions from the growing ice crystals. Upon freezing, salt ions migrate in the concentrated fibroin zones which, once below the eutectic temperature, can crystallize. When freezing is completed, hydrated salt crystals are entrapped within the leaf-like silk fibroin structures. The final washing step leaches the salt, leaving micropores where salt crystals were trapped.

Swelling ratio and water uptake were measured to further characterize the scaffolds (Table 1). For those prepared at −22 °C, the swelling ratio rose from 14.8 to 19.5 and the water uptake from 93.7 to 95.1% in response to concentration of the NaCl solution in the process. This behavior was expected since SEM pictures in Fig. 2 show development of a network containing more porous gaps with increasing salt concentration. Such organization facilitates swelling and water retention. The salt concentration also influenced mechanical properties (Fig. 5). Both the compressive strength and compressive modulus decreased with addition of salt during scaffold processing, in agreement with results of Table 1. Indeed, a higher swelling ratio and water uptake can be expected to correspond to a weaker and more compliant structure. Compression data could not be obtained for scaffolds treated with salt concentration higher than 50 mM because their low values were undetectable with the instrument used. Differences in mechanical strength between scaffolds were thus more pronounced than differences in swelling ratio and water uptake. Salt concentration likewise affected the swelling ratio, water uptake, and

Table 1 Swelling ratio and water uptake values of freeze-dried silk fibroin scaffolds

NaCl concentration (mM)	Swelling ratio		Water uptake (%)	
	−22 °C	−73 °C	−22 °C	−73 °C
0	14.8 ± 0.9	11.8 ± 1.9	93.7 ± 0.3	92.1 ± 1.2
50	15.5 ± 0.7	13.7 ± 0.8	93.9 ± 0.2	93.2 ± 0.3
75	15.6 ± 0.8	14.3 ± 1.5	94.0 ± 0.3	93.4 ± 0.7
100	15.9 ± 0.2	14.6 ± 0.8	94.1 ± 0.1	93.6 ± 0.3
250	19.5 ± 1.9	–	95.1 ± 1.4	–

Values are averages ± standard deviation (N = 3)

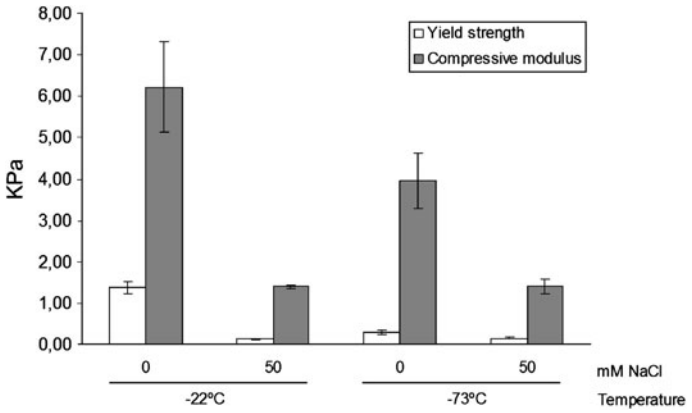

Fig. 5 Mechanical properties of processed scaffolds. Values are averages ± standard deviation ($N = 3$)

mechanical properties of scaffolds processed at −73 °C (Table 1, Fig. 5), although values were always lower with these scaffolds compared to their corresponding −22 °C. The scaffold processed at −73 °C and with 250 mM NaCl was mechanically too weak to give adequate measure of swelling ratio as the matrix easily collapsed, exuding water from the network. Although they show lower swelling capacities (Table 1), the lower values of compressive strength and modulus for the −73 °C scaffolds may be explained by the preferential formation of leaflets over interconnected networks and the presence of more irregularities (micropores and finger-like outgrowths).

Evaluation of the molecular structure of the scaffolds

The secondary structure of silk fibroin in the scaffolds was studied in order to verify the potential effect of the freezing temperature and salt concentration. This was done by FT-IR spectroscopy and XRD. In the last few years, the molecular structure of silk fibroin has been thoroughly investigated in order to fully understand its organization mechanism [19, 42, 43]. Several silk fibroin polymorphs exist and are present in different ratios depending on the silk type and processing methods used. The Silk I structure is not well understood and has been assumed to be a mix of α-helix and random coil conformations [42, 44]. This metastable structure is not desirable in regenerated silk fibroin materials due to its resulting water solubility. Spun silk fibroin is known to have a Silk II structure composed of anti-parallel β-sheets that confer water insolubility [14]. Many routes to induce β-sheet formation in regenerated silk fibroin materials have been explored, including low pH [15, 44], mechanical [32, 44] or solvent [15, 32, 40] treatments, high temperature [45] or water annealing [22], and processing with salts [1, 15]. Among these, the most common approach to convert silk fibroin from a Silk I to Silk II structure is to add polar alcohols such as methanol or ethanol because of its ease of use and efficacy [46].

As shown in Fig. 6a–c, FT-IR spectra of the scaffolds processed at both −22 and −73 °C and not treated with methanol exhibit peaks related to silk I structure at 1,648 (amide I) and 1,235 cm^{-1} (amide III), as reported by Nazarov et al. [6]. The differences between the spectra are not significant enough to indicate a change in molecular structure induced by the freezing regime or by the addition of NaCl. Figure 6d and e shows that the solvent-treated scaffolds adopt a predominant anti-parallel β-sheet conformation with peaks at 1,698 and 1,624 cm^{-1} (amide I), 1,515 cm^{-1} (amide II), and 1,261 cm^{-1} (amide III) [6, 40, 43]. These spectra are quite similar to the spectrum of degummed silk fibroin presented in Fig. 6f, but a shoulder at 1,648 cm^{-1} is still present in the spectra of methanol-treated scaffolds. This can be attributed to the presence of residual silk I conformation in the regenerated fibroin secondary structure.

The information obtained by FT-IR spectroscopy is corroborated by the XRD patterns shown in Fig. 7. The methanol-treated scaffolds prepared at the two different temperatures (c and d) present diffraction patterns similar to that of degummed silk fibroin (e). The crystalline peaks appear at about 24, 20, and 9° and correspond to *d* spacings of 3.7, 4.3, and 9.8 Å, respectively, as reported in literature for a β-sheet conformation in silkworm silk fibroin [40, 43, 47]. The relative intensity of the peaks at 3.7 and 9.8 Å is lower for the solvent-treated scaffolds than for degummed silk fibroin threads. This is a further indication of the presence of residual silk I conformation within the scaffolds, as noted in the FT-IR spectra of Fig. 6. Indeed, the patterns of the non-treated scaffolds (a and b) are dominated by a

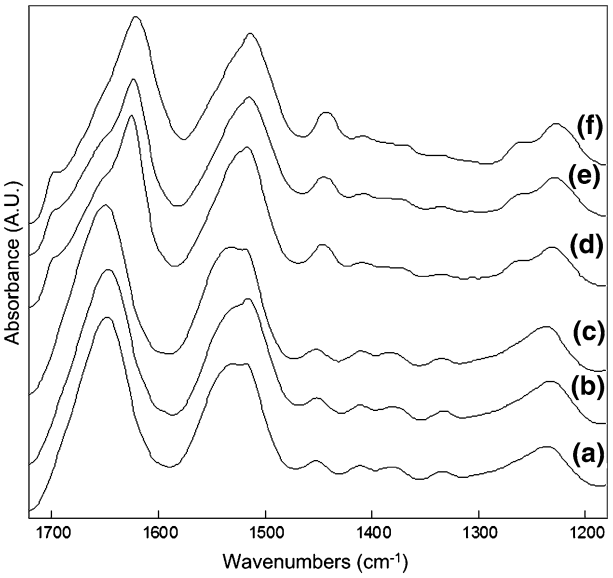

Fig. 6 FT-IR spectra of freeze-dried silk fibroin scaffolds prepared: without methanol treatment nor salt at **a** −73 °C and **b** −22 °C, **c** without methanol treatment and with 250 mM NaCl at −22 °C, **d** with methanol treatment and without salt at −73 °C and **e** with methanol treatment and without salt at −22 °C. Spectrum f represents degummed silk fibroin threads

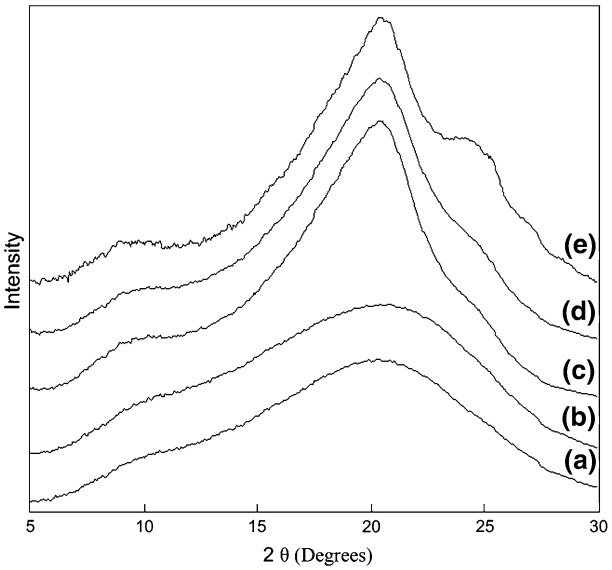

Fig. 7 X-ray diffraction patterns of freeze-dried silk fibroin scaffolds (no added salt) without (**a**, **b**) and with a methanol treatment (**c**, **d**). Scaffolds were prepared at −73 °C for patterns **a** and **c** and at −22 °C for **b** and **d**. Pattern **e** represents degummed silk fibroin threads

diffuse halo centered at approximately 20° (4.3 Å). Since methanol was added after freeze-drying the samples, the molecular changes induced by methanol treatment may be only partial because of the lack of mobility of protein chains in the solid state. Finally, there is no evidence for a change in molecular structure induced by a modification of the freezing regime (Fig. 7a, b) or by the presence of NaCl in the solution (data not shown).

P19 cell culture in fibroin scaffolds

Numerous studies have already established the biocompatibility of silk fibroin scaffolds with cell culture by assaying the viability and the proliferation of various cell types [48]. However, comparisons of the distribution of cells within these scaffolds have rarely been done. Cell distributions have been examined, for example, in fibroin–chitosane constructs [49]. Given the two distinct morphologies of our scaffolds (sponge-like interconnected networks and leaflet stacks), we examined whether one or the other morphology favored cell penetration into the scaffold and whether the presence of salt in the solution was influential. The mouse P19 embryonic carcinoma cells were used in this series of experiments. These embryonic stem cells, often studied as a model of cell differentiation, have different spatial needs whether they are propagated as undifferentiated individual cells or are aggregated as multicellular spheroids to induce their differentiation into various cell types such as neurons and cardiomyocytes [50, 51]. The P19 cells were seeded onto the different silk fibroin scaffolds and imaged 24 h later using scanning confocal

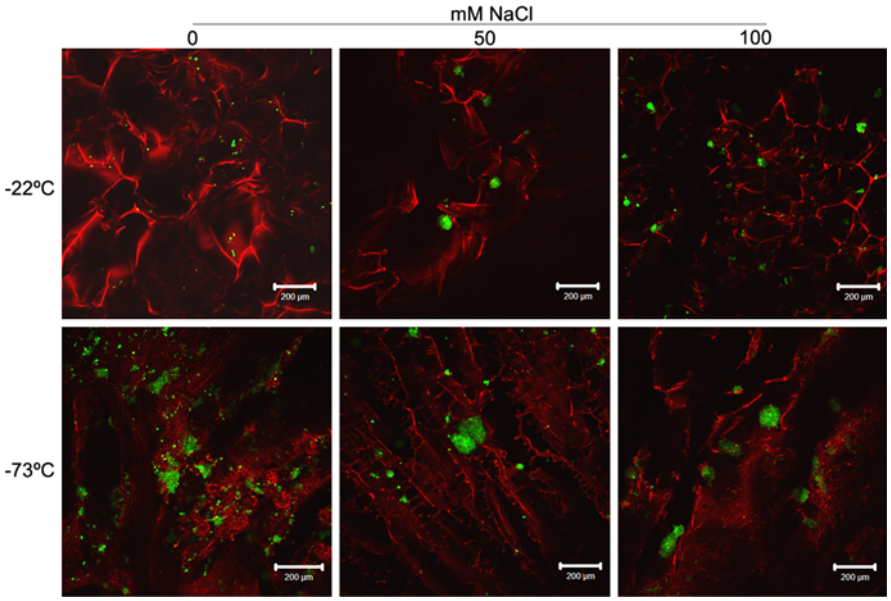

Fig. 8 Confocal microscopy images of P19 cells seeded in freeze-dried silk fibroin scaffolds. Cells were labeled with CFSE to permit their visualization by green fluorescence. A second staining with propidium iodide, done at the end of the culture, tinted the scaffold matrix in brilliant red, allowing the visualization of both cells and matrix. Propidium iodide also marked dead cells (which appeared as *yellowish fluorescent dots*). Images show cell distribution at the surface of scaffolds (at the cell-seeded side). (Color figure online)

microscopy. Cells were loaded with the green fluorescent CFSE dye before seeding to follow their distribution in the scaffolds. The scaffold/cells systems were loaded with propidium iodide dye before microscopy (that is, 24 h post-seeding). This red fluorescent dye stained the scaffold matrix in brilliant red, allowing the combined visualization of cells and matrix. Propidium iodide also gave an orange color to dead cells labeled with CFSE, allowing the verification of cell viability. Less than 10% of cells escaped the scaffolds and grew on the plastic surface of culture wells by comparing with wells not containing scaffolds. Almost all cells remained alive after their seeding onto the biomaterials. Indeed, there were very rare orange spots on photomicrographs, as illustrated in Fig. 8, and there were almost no floating cells in the culture supernatants.

The freezing conditions and salt concentration affected the colonization of the scaffolds by cells. Figure 8 shows the cell distribution at the scaffold surface. The −73 °C/no salt scaffold exhibited numerous cells, mostly individual, on its surface. The −22 °C/no salt scaffold also showed individual cells although the number was greatly diminished. On the contrary, cells assembled into aggregates on scaffolds processed at either temperature in the presence of salt. Pores created by salt thus acted as niches that can accommodate many cells for subsequent aggregation. Furthermore, the budding features within the −73 °C/salt processed scaffolds likely provided anchor points for cell clustering. We then determined whether the

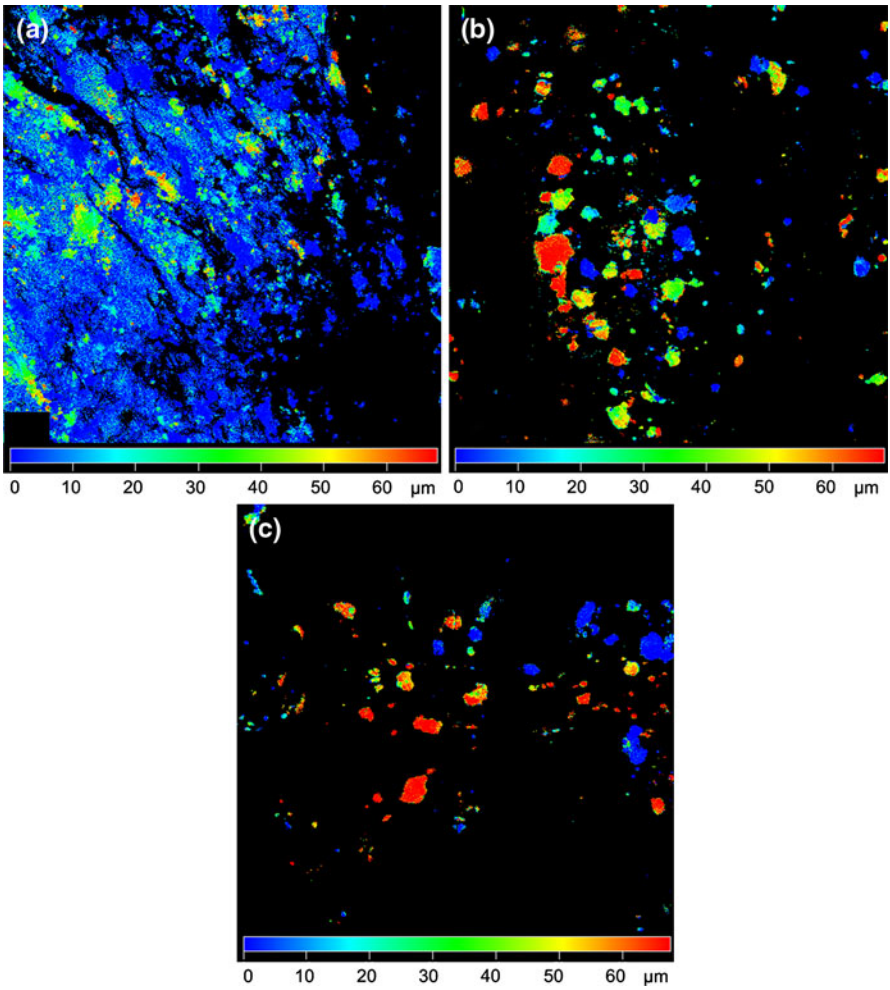

Fig. 9 Reconstituted 3D confocal microscopy images illustrating the capacity of P19 cells to penetrate into scaffolds processed without NaCl at −73 °C (**a**), and with 50 mM NaCl at −73 and −22 °C (**b**, **c**, respectively). The green CFSE fluorescence was color-coded as a function of the distance of the fluorescing cells within the scaffold, from 0 (*blue*) to 60 μm (*red*), with the slide surface being at 0 μm. The penetration profiles of the other scaffolds resembled those of **b** and **c**. (Color figure online)

processing conditions influenced cell penetration into the scaffolds. Figure 9 shows that high cell density at the surface of the −73 °C/no salt scaffold correlated with low penetration. The closely packed fibroin leaflets of this scaffold may have hindered cell penetration and aggregation. In contrast, the use of NaCl solution, which increased the swelling ratio and created micropores, favored both phenomena. The budding features may preserve the housing spaces by preventing the collapse of fibroin leaflets. Cells found deeply in the scaffold were alive, in agreement with the known biocompatibility of silk fibroin. The viability of these cells attested the efficient mass transfer of nutrients and waste across the scaffolds.

Formation of cell aggregates in the scaffolds is an interesting finding considering the importance of aggregation in the differentiation of P19 cells. In addition, the size of the cell aggregates formed within the scaffolds were comparable to those prepared in Petri dishes, suggesting that differentiation could be effective in the scaffolds.

Conclusions

This study showed that the physical aspect of 3D silk fibroin scaffolds can be efficiently tuned by varying simultaneously the freezing temperature and salt concentration of the biopolymer slurries. Slow freezing at −22 °C generated sponge-like networks with interconnected pores, a morphology obtained under a large variety of conditions. However, the formation of multilayered silk fibroin scaffolds with stacked leaflets, such as those we obtained by fast freezing at −73 °C, has seldom been reported in the literature. The multilayered scaffolds could find applications for cell cultures requiring cell alignment. This work also showed that the matrix microporosity can be modified with salt concentration, thus affecting the swelling ratio and the mechanical properties of the scaffolds. In addition, the presence of salt in the fast-frozen fibroin solutions generated finger-like structures which, together with the micropores, can modulate the dimensions of the cell housing spaces within the scaffolds. Indeed, the use of NaCl solutions promoted penetration as well as aggregation of the P19 cells. The relative simplicity of this methodology opens the way for a morphological template optimization of silk fibroin scaffolds that could be designed for a variety of cell support applications including oriented cell cultures and preparation of porous tissues.

Acknowledgments We are grateful to R. Mineau and D. Flipo for their help with the SEM and scanning confocal microscopy images, respectively. We are also very thankful to D.L. Kaplan and J.A. Kluge (Tufts University) for their kind assistance with the mechanical testing. F.B. thanks Pharmaqam for the award of a scholarship. This work was partly supported by grants from the Natural Sciences and Engineering Research Council of Canada (I.M., C.P. and M.A.M) and the Canadian Institutes for Health Research (J.P.).

References

1. Kim U-J, Park J, Joo Kim H, Wada M, Kaplan DL (2005) Three-dimensional aqueous-derived biomaterial scaffolds from silk fibroin. Biomaterials 26(15):2775–2785
2. Agrawal CM, Ray RB (2001) Biodegradable polymeric scaffolds for musculoskeletal tissue engineering. J Biomed Mater Res 55(2):141–150
3. Zmora S, Glicklis R, Cohen S (2002) Tailoring the pore architecture in 3-D alginate scaffolds by controlling the freezing regime during fabrication. Biomaterials 23(20):4087–4094
4. Hollister SJ (2005) Porous scaffold design for tissue engineering. Nat Mater 4(7):518–524
5. Hofmann S, Hagenmüller H, Koch AM, Müller R, Vunjak-Novakovic G, Kaplan DL, Merkle HP, Meinel L (2007) Control of in vitro tissue-engineered bone-like structures using human mesenchymal stem cells and porous silk scaffolds. Biomaterials 28(6):1152–1162
6. Nazarov R, Jin H-J, Kaplan DL (2004) Porous 3-D scaffolds from regenerated silk fibroin. Biomacromolecules 5(3):718–726
7. Sofia S, McCarthy MB, Gronowicz G, Kaplan DL (2001) Functionalized silk-based biomaterials for bone formation. J Biomed Mater Res 54(1):139–148

8. Budyanto L, Goh Y, Ooi C (2009) Fabrication of porous poly(L-lactide) (plla) scaffolds for tissue engineering using liquid–liquid phase separation and freeze extraction. J Mater Sci Mater Med 20(1):105–111
9. Madihally SV, Matthew HWT (1999) Porous chitosan scaffolds for tissue engineering. Biomaterials 20(12):1133–1142
10. Liu CZ, Xia ZD, Han ZW, Hulley PA, Triffitt JT, Czernuszka JT (2008) Novel 3D collagen scaffolds fabricated by indirect printing technique for tissue engineering. J Biomed Mater Res Part B 85B(2):519–528
11. Hu Y, Grainger DW, Winn SR, Hollinger JO (2002) Fabrication of poly(alpha-hydroxy acid) foam scaffolds using multiple solvent systems. J Biomed Mater Res 59(3):563–572
12. Stokols S, Tuszynski MH (2004) The fabrication and characterization of linearly oriented nerve guidance scaffolds for spinal cord injury. Biomaterials 25(27):5839–5846
13. Lee KY, Mooney DJ (2001) Hydrogels for tissue engineering. Chem Rev 101(7):1869–1880
14. Altman GH, Diaz F, Jakuba C, Calabro T, Horan RL, Chen J, Lu H, Richmond J, Kaplan DL (2003) Silk-based biomaterials. Biomaterials 24(3):401–416
15. Vepari C, Kaplan DL (2007) Silk as a biomaterial. Prog Polym Sci 32(8–9):991–1007
16. Mandal BB, Kundu SC (2009) Cell proliferation and migration in silk fibroin 3D scaffolds. Biomaterials 30(15):2956–2965
17. Perasso R, Zhou CZ, Li ZG, Confalonieri F, Medina N, Zivanovic Y, Esnault C, Yang T, Jacquet M, Janin J, Duguet M (2000) Fine organization of bombyx mori fibroin heavy chain gene. Nucleic Acids Res 28:2413–2419
18. Inoue S, Tanaka K, Arisaka F, Kimura S, Ohtomo K, Mizuno S (2000) Silk fibroin of bombyx mori is secreted, assembling a high molecular mass elementary unit consisting of h-chain, l-chain, and p25, with a 6:6:1 molar ratio. J Biol Chem 275(51):40517–40528
19. Shen Y, Johnson MA, Martin DC (1998) Microstructural characterization of bombyx mori silk fibers. Macromolecules 31(25):8857–8864
20. Servoli E, Maniglio D, Motta A, Predazzer R, Migliaresi C (2005) Surface properties of silk fibroin films and their interaction with fibroblasts. Macromol Biosci 5(12):1175–1183
21. Horan RL, Antle K, Collette AL, Wang Y, Huang J, Moreau JE, Volloch V, Kaplan DL, Altman GH (2005) In vitro degradation of silk fibroin. Biomaterials 26(17):3385–3393
22. Lawrence BD, Cronin-Golomb M, Georgakoudi I, Kaplan DL, Omenetto FG (2008) Bioactive silk protein biomaterial systems for optical devices. Biomacromolecules 9(4):1214–1220
23. Lawrence BD, Marchant JK, Pindrus MA, Omenetto FG, Kaplan DL (2009) Silk film biomaterials for cornea tissue engineering. Biomaterials 30(7):1299–1308
24. Hino T, Tanimoto M, Shimabayashi S (2003) Change in secondary structure of silk fibroin during preparation of its microspheres by spray-drying and exposure to humid atmosphere. J Colloid Interface Sci 266:68–73
25. Zhu J, Shao H, Hu X (2007) Morphology and structure of electrospun mats from regenerated silk fibroin aqueous solutions with adjusting ph. Int J Biol Macromol 41(4):469–474
26. Li C, Vepari C, Jin H-J, Kim HJ, Kaplan DL (2006) Electrospun silk-bmp-2 scaffolds for bone tissue engineering. Biomaterials 27(16):3115–3124
27. Li M, Wu Z, Zhang C, Lu S, Yan H, Huang D, Ye H (2001) Study on porous silk fibroin materials. II. Preparation and characteristics of spongy porous silk fibroin materials. J Appl Polym Sci 79(12):2192–2199
28. Uebersax L, Merkle HP, Meinel L (2008) Insulin-like growth factor I releasing silk fibroin scaffolds induce chondrogenic differentiation of human mesenchymal stem cells. J Control Rel 127(1):12–21
29. Tamada Y (2005) New process to form a silk fibroin porous 3-D structure. Biomacromolecules 6(6):3100–3106
30. Zhang H, Cooper AI (2007) Aligned porous structures by directional freezing. Adv Mater 19(11):1529–1533
31. Kwon S-M, Kim H-S, Jin H-J (2009) Multiwalled carbon nanotube cryogels with aligned and non-aligned porous structures. Polymer 50(13):2786–2792
32. Ishida M, Asakura T, Yokoi M, Saito H (2002) Solvent- and mechanical-treatment-induced conformational transition of silk fibroins studies by high-resolution solid-state carbon-13 NMR spectroscopy. Macromolecules 23(1):88–94
33. Bouchard F, Paquin J (2009) Skeletal and cardiac myogenesis accompany adipogenesis in p19 embryonal stem cells. Stem Cells Dev 18(7):1023–1032

34. Fukasawa T, Deng ZY, Ando M, Ohji T, Goto Y (2001) Pore structure of porous ceramics synthesized from water-based slurry by freeze-dry process. J Mater Sci 36(10):2523–2527
35. Vrbka L, Jungwirth P (2007) Molecular dynamics simulations of freezing of water and salt solutions. J Mol Liq 134(1–3):64–70
36. Carignano MA, Baskaran E, Shepson PB, Szleifer I (2006) Molecular dynamics simulation of ice growth from supercooled pure water and from salt solution. Ann Glaciol 44:113–117
37. Vrbka L, Jungwirth P (2005) Brine rejection from freezing salt solutions: a molecular dynamics study. Phys Rev Lett 95(14):148501
38. Hu K, Cui F, Lv Q, Ma J, Feng Q, Xu L, Fan D (2008) Preparation of fibroin/recombinant human-like collagen scaffold to promote fibroblasts compatibility. J Biomed Mater Res Part A 84A(2):483–490
39. Zaritzky N (2005) Physical-chemical principles in freezing. In: Sun D-W (ed) Handbook of frozen food processing and packaging. Taylor and Francis group edn. CRC Press, Boca Raton, FL, pp 3–32
40. Nam J, Park YH (2001) Morphology of regenerated silk fibroin: Effects of freezing temperature, alcohol addition, and molecular weight. J Appl Polym Sci 81(12):3008–3021
41. Nam YS, Park TG (1999) Biodegradable polymeric microcellular foams by modified thermally induced phase separation method. Biomaterials 20(19):1783–1790
42. Marsh RE, Corey RB, Pauling L (1955) An investigation of the structure of silk fibroin. Biochim Biophys Acta 16:1–34
43. Asakura T, Kuzuhara A, Tabeta R, Saito H (2002) Conformational characterization of bombyx mori silk fibroin in the solid state by high-frequency carbon-13 cross polarization-magic angle spinning NMR, X-ray diffraction, and infrared spectroscopy. Macromolecules 18(10):1841–1845
44. He S-J, Valluzzi R, Gido SP (1999) Silk I structure in bombyx mori silk foams. Int J Biol Macromol 24(2–3):187–195
45. Lv Q, Cao C, Zhang Y, Ma X, Zhu H (2005) Preparation of insoluble fibroin films without methanol treatment. J Appl Polym Sci 96(6):2168–2173
46. Chen X, Shao Z, Marinkovic NS, Miller LM, Zhou P, Chance MR (2001) Conformation transition kinetics of regenerated bombyx mori silk fibroin membrane monitored by time-resolved ftir spectroscopy. Biophys Chem 89(1):25–34
47. Sashina E, Bochek A, Novoselov N, Kirichenko D (2006) Structure and solubility of natural silk fibroin. Russ J Appl Chem 79(6):869–876
48. Velema J, Kaplan D (2006) Biopolymer-based biomaterials as scaffolds for tissue engineering. In: Lee K, Kaplan D (eds) Tissue engineering I. Advances in biochemical engineering/biotechnology, vol 102. Springer, Berlin, Heidelberg, pp 187–238
49. Chung T-W, Chang Y-L (2010) Silk fibroin/chitosan–hyaluronic acid versus silk fibroin scaffolds for tissue engineering: promoting cell proliferations in vitro. J Mater Sci Mater Med 21(4):1343–1351
50. Skerjanc IS (1999) Cardiac and skeletal muscle development in p19 embryonal carcinoma cells. Trends in Cardiovascul Med 9(5):139–143
51. Rudnicki MA, McBurney MW (1987) Cell culture methods and induction of differentiation of embryonal carcinoma cell lines. In: Robertson EJ (ed) Teratocarcinomas and embryonic stem cells: a practical approach. IRL press edn. IRL Press, Oxford, pp 19–49